Two-dimensional solitons in a quintic-septimal medium

Albert S. Reyna,* Kelly C. Jorge, and Cid B. de Araújo
Departamento de Física, Universidade Federal de Pernambuco, 50670-901 Recife, PE, Brazil
(Received 28 September 2014; published 24 December 2014)

We report an observation of spatial solitons in a medium managed to present fifth-seventh (focusing-defocusing) refractive nonlinearities with suppressed third-order nonlinearity. Propagation of two-dimensional bright spatial solitons for ∼10 Rayleigh lengths was observed and characterized in a suspension of silver nanoparticles in acetone using the scattered light imaging method. Numerical calculations based on a nonlinear Schrödinger-type equation, including contributions up to the seventh-order susceptibility, were performed showing good agreement with the experimental results.

DOI: 10.1103/PhysRevA.90.063835 PACS number(s): 42.65.Tg, 42.65.An, 42.65.Jx

I. INTRODUCTION

The study of nonlinear (NL) phenomena induced by laser pulses propagating in transparent media is a complex subject of great interest. For moderate laser intensities the NL propagation of light is understood in terms of the optical Kerr effect which describes light-induced changes in the materials' refractive index that may lead to beam self-focusing, spectral broadening, and several other NL phenomena [1]. For large light intensities the optical response is affected by saturation of the Kerr effect and high-order nonlinearities (HONs) may induce optical phenomena such as multiphoton absorption and change of the refractive index due to plasma formation [2]. Although for some applications (such as ultrafast optical switching in solids) HON may cause problems, in several cases their contributions are very important and desired. For instance, HON may enable formation of stable solitons in homogeneous isotropic media [3] and influence many aspects of filamentation in gases and condensed matter [4]. HON-assisted phenomena such as liquid light condensates [5], harmonic conical diffraction [6], and filamentation [2,4,7] are largely studied with basis on the NL interaction of light with various physical systems. Also of great interest is the exploitation of HON for quantum information [8], quantum memories [9], and for coherence quantum control [10]. From the theoretical point of view analogies between superfluids [11], plasmas [12], and Bose-Einstein condensates [13] can be evaluated from the behavior of highly NL optical systems. In studies related to the phenomena mentioned above, several authors devoted special attention to the concept of nonlinearity management which also inspired large activity in theoretical physics and mathematics research [14]. In the present work the management of HON is performed to investigate the formation of optical spatial solitons.

Spatial solitons are self-trapped optical beams that propagate with invariant shape due to a balance between linear diffraction and NL interaction with the medium where they propagate [15–18]. Various kinds of spatial solitons supported by different types of nonlinearities were studied since the report of self-trapping of optical beams in [15], aiming to be implemented for applications such as optical interconnects [19], image transmission [20], and waveguides for optical communication devices [21]. In particular, the observation of (1+1)-dimensional [(1+1)D] spatial solitons was reported in [22] and their behavior is described by the cubic NL Schrödinger equation. However, the stable propagation of two-dimensional [(2+1)D] spatial solitons is not supported in homogeneous isotropic media with instantaneous cubic nonlinearity (Kerr media), due to catastrophic self-focusing [23]. Nevertheless, HONs are manifested in media with large NL susceptibility allowing arrest of the catastrophic beam collapse. Indeed, the propagation of stable (2+1)D spatial solitons was reported in a glass presenting large three-photon absorption (3PA) cross section [24]. More recently, there was a report of the propagation of stable (2+1)D spatial solitons in liquid CS_2 due to the simultaneous contributions of third- and fifth-order susceptibilities, $\chi^{(3)}$ and $\chi^{(5)}$, respectively [25]. The theoretical description based on the cubic-quintic NL Schrödinger equation including 3PA showed good agreement with the experimental results. The opposite signs of $\mathrm{Re}\chi^{(3)} > 0$ and $\mathrm{Re}\chi^{(5)} < 0$, as well as the contribution of $\mathrm{Im}\chi^{(5)} > 0$, were the ingredients that allowed the observation of robust bright spatial soliton propagation for a long distance.

Unfortunately, homogeneous systems do not allow easy control of HON in order to suppress or enhance particular NL contributions. On the other hand, nonlinearity management of nanocomposites enables the control of effects associated with NL susceptibilities of different order [26,27]. The effective susceptibilities of a nanocomposite, $\chi_{\mathrm{eff}}^{(2N+1)}$, $N = 1, 2, 3, \ldots$, contain information related to the host medium and to the nanoparticles (NPs) through their respective NL susceptibilities that contribute for the total response according to the volume fraction of the NPs.

HONs of colloids containing silver NPs suspended in liquids were reported in [28] and the NL parameters determined have been considered in theoretical papers that proposed the observation of many NL effects in systems with quintic and cubic-quintic nonlinearity [29]. The experimental observation of interesting effects, such as spatial-modulation instability due to pure $\chi_{\mathrm{eff}}^{(5)}$, and spatial-phase modulation due to $\chi_{\mathrm{eff}}^{(5)}$ and $\chi_{\mathrm{eff}}^{(7)}$, was possible thanks to nonlinearity management of metal-dielectric nanocomposites [26,27]. Therefore, metal colloids are strong candidates for demonstration of unique optical effects. Indeed, varying the volume fraction, f, of the metallic NPs in a colloid it is possible to suppress or enhance the contribution of a specific nonlinearity. In

*Corresponding author: areynao@yahoo.com.br

particular, for silver NPs in acetone, when $f = 1.6\times10^{-5}$, the third-order refractive nonlinearity is suppressed due to the opposite NL contributions of the host and the NPs. This result is independent of the laser intensity but depends on the laser frequency through the dielectric functions of the nanocomposite constituents [26,27].

In the present paper we exploit the procedure presented in [26,27] and report the propagation of spatial solitons in a quintic-septimal nanocomposite. By varying the volume fraction of silver NPs suspended in acetone it was possible to manage the colloid NL response to obtain $\mathrm{Re}\chi^{(3)}_{\mathrm{eff}} = 0$, $\mathrm{Re}\chi^{(5)}_{\mathrm{eff}} > 0$, and $\mathrm{Re}\chi^{(7)}_{\mathrm{eff}} < 0$, and to observe the propagation of (2+1)D bright spatial solitons. Robust spatial solitons propagating by ∼10 Rayleigh lengths were observed due to simultaneous contributions of the fifth- and seventh-order susceptibilities using the scattered light imaging method (SLIM) [30]; the behavior of the propagating optical pulses was described by numerical solution of the cubic-quintic-septimal nonlinear Schrödinger-type equation with appropriate relative contributions of $\chi^{(2N+1)}_{\mathrm{eff}}$, $N = 1-3$, for different f values. When $f = 1.6\times10^{-5}$ the propagation equation reduces to the quintic-septimal NL Schrödinger-type equation, also including the imaginary parts of the susceptibilities.

II. EXPERIMENTAL DETAILS

The samples containing silver NPs were synthesized according to the methods described in [28,31]. Colloids with $f = 0.5\times10^{-5}$, 1.6×10^{-5}, and 2.5×10^{-5} were prepared by adding 20, 33, and 43 μl of the Ag NP-water suspension in 1 ml of acetone. The linear absorption spectra of the samples were typical of colloids with silver NPs presenting the localized surface plasmon resonance (LSPR) at ∼400 nm [26–28,32]. The measured LSPR linewidth of ∼50 nm indicated that the samples prepared have homogeneous NP size distribution and this was corroborated by transmission electronic microscopy that identified an average diameter of (9.0 ± 2.2) nm. The NL refractive indices, $n_{2N} \propto \mathrm{Re}\chi^{(2N+1)}_{\mathrm{eff}}$, and NL absorption coefficients, $\alpha_{2N} \propto \mathrm{Im}\chi^{(2N+1)}_{\mathrm{eff}}$, were measured applying the Z-scan technique using the setup described in [26,27]; their behavior as a function of f was linear, as in the previous measurements [26–28].

The experimental setup for investigation of bright spatial solitons is illustrated in Fig. 1. The second harmonic of a Q-switched and mode-locked Nd:YAG laser (80 ps, 10 Hz, 532 nm) with maximum pulse energy of 10 μJ was used. The control of the incident beam power on the sample was made with a $\lambda/2$ plate followed by a Glan prism. A spatial filter was used to obtain a beam with a nearly Gaussian spatial profile corresponding to the beam quality factor $M^2 = 1.1$. The metal-colloid sample was contained in a quartz cell (length: 10 mm). A 1-cm focal length lens was used to focus the beam at the input face of the quartz cell, producing a beam waist of ∼7 μm with Rayleigh length of ∼0.25 mm.

The spatial profile of the propagating beam along the sample was characterized following two complementary procedures. The first procedure was used in [25,33] and consists in capturing the transverse profile of the beam emerging from the sample by placing a charge-coupled device (CCD) camera

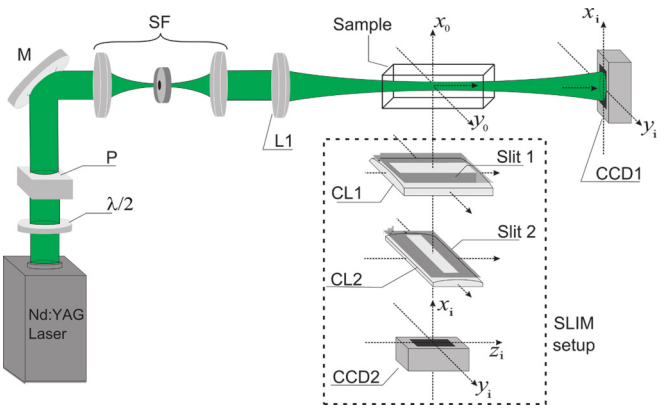

FIG. 1. (Color online) Experimental setup. Polarizer (P); mirror (M); spatial filter (SF); spherical lens with $f = 10$ mm (L1). The CCD1 camera was used to obtain the transmitted beam spatial profile. Cylindrical lenses with $f = 40$ mm (CL1) and $f = 80$ mm (CL2), and CCD2 were used in the SLIM setup. Sample length: 10 mm.

(1360×1024 pixels) in the far-field region, aligned with the beam-propagation axis. The second procedure was based on the scattered light imaging method (SLIM) [30]. This method allows the observation and characterization of the beam propagation inside the sample by monitoring the light scattered in the direction perpendicular to the beam axis. To perform measurements an imaging optical system, consisting of two cylindrical lenses oriented with orthogonal axes and a CCD camera, were used as shown in Fig. 1. Lenses with 40-mm and 80-mm focal lengths focusing on the y axis (transverse direction) and z axis (the beam-propagation direction) were used to obtain an image magnification of 7 and $\frac{1}{2}$, respectively. More details on the imaging system are given in [30].

III. RESULTS AND DISCUSSION

The experiments were performed with various laser intensities to investigate the formation of the bright spatial solitons.

Figures 2(a)–2(c) summarize the beam radius measurements obtained according to the first procedure as a function of the incident intensity. The data were collected after the beam passed through a 2-mm-long sample. A telescope with magnification of 5 was placed in front of the CCD camera in order to obtain an image of the exit plane of the sample over a large detection area. The black dots represent the experimental data while the red lines were obtained by solving the NL propagation equation as described below. For $I \leqslant 10$ GW/cm^2 the beam radius does not change much for the three volume fractions and its value is equal to that of a beam propagating in a linear host medium with linear refractive index equal to 1.36; the small changes are only due to the linear diffraction. For $I > 10$ GW/cm^2 a gradual decrease in the beam radius size is observed due to the samples' nonlinearity, reaching a minimum radius for $I \approx 60$ GW/cm^2, as shown in Figs. 2(b) and 2(c). The minimum radius reached, $w \approx 7$ μm, is equal to the input beam waist. The behavior shown in Fig. 2(b), where a beam waist remains constant for $I \geqslant 60$ GW/cm^2, indicates the formation of stable spatial solitons.

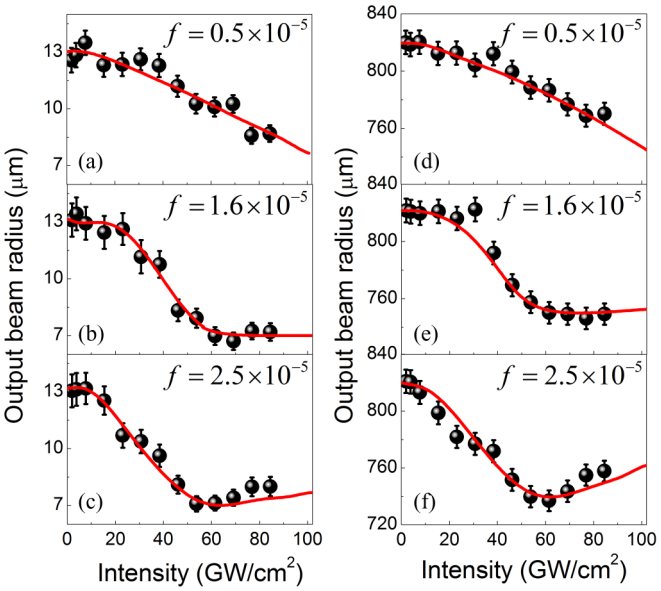

FIG. 2. (Color online) Dependence of the transmitted laser beam radius as a function of the input intensity for (a) $f_1 = 0.5\times10^{-5}$, (b) $f_2 = 1.6\times10^{-5}$, and (c) $f_3 = 2.5\times10^{-5}$ using a 2-mm-long cell. A CCD camera acquired the beam profile at the output face of the cell; for (d) f_1, (e) f_2, and (f) f_3 using a 1-cm-long cell. The CCD camera was placed 7 cm away from the output face. The red solid lines represent theoretical results obtained from Eq. (1) taking into account the beam diffraction in the propagation from the cell to the camera.

Figures 2(d)–2(f) show similar results using a 1-cm-long sample. The CCD camera was placed 7 cm away from the exit face of the cell to exploit a large detection area. A similar behavior of the beam radius as a function of the incident intensity was observed for the three volume fractions, with minimum beam radius of $w \approx 750\ \mu$m, recorded by the camera positioned in the far-field region, for $I \approx 60$ GW/cm^2. Numerical results were obtained by solving the NL propagation equation using the parameters determined by Z-scan measurements for each f value, considering a light propagation distance of 2 mm inside the cell corresponding to Figs. 2(a)–2(c); the results shown in Figs. 2(d)–2(f) were obtained by considering the light propagation inside the 10-mm cell and 7 cm in the free space where the beam suffers only linear diffraction.

The results shown in Figs. 2(a) and 2(d) for $I <$ 20 GW/cm^2 are essentially due to $\chi^{(3)}_{\rm eff}$ while Figs. 2(b) and 2(e) correspond to a colloid with NL behavior dominated by $\mathrm{Re}\chi^{(5)}_{\rm eff} > 0$ and $\mathrm{Re}\chi^{(7)}_{\rm eff} < 0$, with $\mathrm{Re}\chi^{(3)}_{\rm eff} = 0$. Figures 2(c) and 2(f) show results contributed by $\chi^{(3)}_{\rm eff}$, $\chi^{(5)}_{\rm eff}$, and $\chi^{(7)}_{\rm eff}$, as characterized in [26,27]. For intensities larger than 20 GW/cm^2 the contribution of $\chi^{(7)}_{\rm eff}$ becomes relevant in all cases illustrated by Fig. 2. The corresponding values of the effective NL parameters, determined using the Z-scan technique, were $n_2 = +1.7\times10^{-15}$ cm^2/W, $n_4 = +1.3\times10^{-25}$ cm^4/W^2, and $n_6 = -2.0\times10^{-35}$ cm^6/W^3 for $f = 0.5\times10^{-5}$; $n_2 = 0$, $n_4 = +3.2\times10^{-25}$ cm^4/W^2, and $n_6 = -7.0\times10^{-35}$ cm^6/W^3 for $f = 1.6\times10^{-5}$; and $n_2 = -1.3\times10^{-15}$ cm^2/W, $n_4 = +7.0\times10^{-25}$ cm^4/W^2, and $n_6 = -1.1\times10^{-34}$ cm^6/W^3 for $f = 2.5\times10^{-5}$.

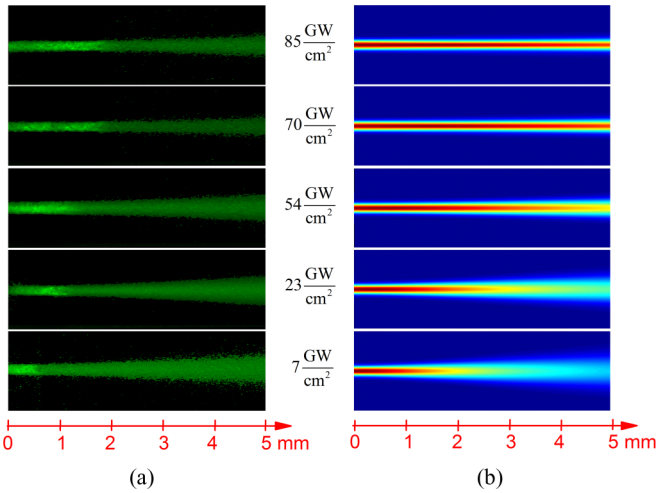

FIG. 3. (Color online) Transverse beam images: (a) experimental data obtained using the SLIM and (b) numerical results obtained from Eq. (1), for $f = 1.6\times10^{-5}$.

Figure 3(a) shows transverse beam images for $f = 1.6\times10^{-5}$ with intensities varying from 7 GW/cm^2 to 85 GW/cm^2, obtained using the SLIM. Notice the formation of bright solitons for intensities higher than 20 GW/cm^2 reaching a maximum propagation distance for $I \geqslant 70$ GW/cm^2.

In order to describe the laser beam propagation we solved numerically the NL equation given by

$$2ik\frac{\partial E}{\partial z} + \Delta E = -\frac{\omega^2}{c^2}\left[3\chi^{(3)}_{\rm eff}|E|^2E + 10\chi^{(5)}_{\rm eff}|E|^4E + 35\chi^{(7)}_{\rm eff}|E|^6E\right], \quad (1)$$

where E is the optical field amplitude, Δ is the transverse Laplacian operator, z is the propagation direction, $k = 2\pi n_0/\lambda$, λ is the laser wavelength, n_0 is the linear refractive index, ω is the laser frequency, and c is the speed of light in vacuum. Linear losses were ignored due to the linear absorption coefficient α_0, at 532 nm for the three volume fractions discussed above, are approximately two orders of magnitude smaller than the contributions of $\alpha_{2N}I^N$ with $N = 1, 2, 3$, for the intensities studied. The expression inside brackets on the right-hand side of Eq. (1) represents the total effective NL susceptibility with the numerical coefficients due to the degeneracy factors for the ith-order process [34]. The values of $\chi^{(3)}_{\rm eff} = -i\,6.3\times10^{-22}$ (m^2/V^2) and $\chi^{(5)}_{\rm eff} = +3.7\times10^{-38} + i\,3.3\times10^{-37}$ (m^4/V^4), for $f = 1.6\times10^{-5}$, were obtained from previous experiments [26,27]. For $I \leqslant 20$ GW/cm^2 the contributions of $n_6 \propto \mathrm{Re}\chi^{(7)}_{\rm eff}$ and $\alpha_6 \propto \mathrm{Im}\chi^{(7)}_{\rm eff}$ were negligible in comparison with the third- and fifth-order contributions. For $I > 20$ GW/cm^2, the seventh-order susceptibility becomes relevant and corresponds to $\chi^{(7)}_{\rm eff} = (-4.2 - i\,3.5)\times10^{-54}$ (m^6/V^6) [27].

Figure 3(b) shows the numerical results obtained by solving Eq. (1), using the split-step compact finite difference method [35] for the five laser intensities corresponding to Fig. 3(a).

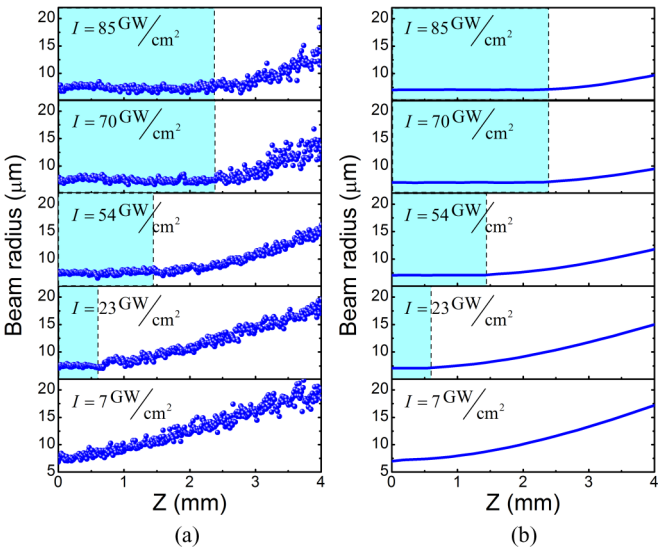

FIG. 4. (Color online) (a) Experimental and (b) theoretical beam radius as a function of propagation distance obtained from Fig. 3. The shaded areas indicate the region of stable soliton propagation ($f = 1.6\times10^{-5}$).

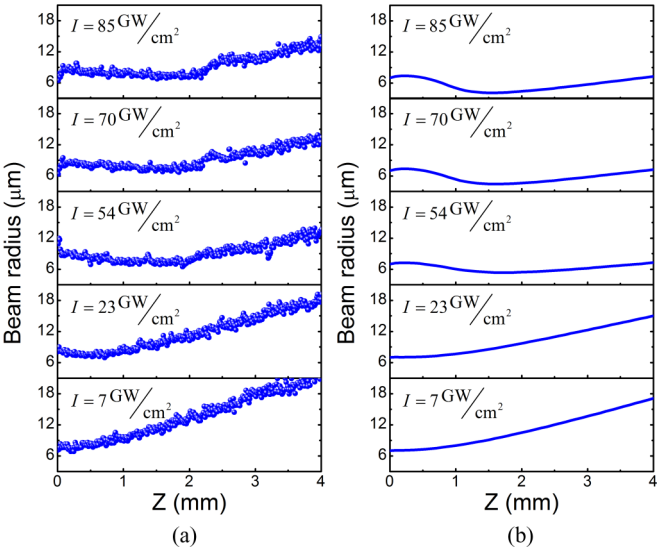

FIG. 5. (Color online) (a) Experimental and (b) theoretical beam radius as a function of propagation distance for $f = 2.5\times10^{-5}$.

The agreement between the numerical and the experimental results corroborates the observation of (2+1)D stable soliton propagation with maximum propagation distance for $I \geqslant 70$ GW/cm^2.

Figure 4 shows the variation of the laser beam radius along the pathway inside the sample with $f = 1.6\times10^{-5}$, determined from the images of Fig. 3, using the SLIM [30]. The experimental results in Fig. 4(a) clearly show that as the laser intensity increases, the propagation distance at which the beam waist remains constant also increases. The maximum propagation distance of ∼2.3 mm corresponding to ∼10 Rayleigh lengths was observed at the highest input intensities. The good agreement between the experimental and theoretical results can be observed comparing the shaded rectangles drawn in Figs. 4(a) and 4(b).

Results of similar measurements and analysis for $f = 2.5\times10^{-5}$ are shown in Fig. 5. According to the model introduced in [27], soliton propagation was not observed for intensities between 3 and 85 GW/cm^2 due to the negative third-order refractive index that dominates the NL response. Notice that Fig. 5(a) for $I \geqslant 54$ GW/cm^2 shows a change in the laser beam radius followed by formation of a new focus around of $z = 2$ mm; Fig. 5(b), obtained solving Eq. (1), displays similar behavior.

For $f = 0.5\times10^{-5}$ the scattered light intensity was very weak and transverse beam images based on the SLIM were not acquired because of the low sensitivity of the CCD camera.

IV. SUMMARY

In summary, we reported the observation and characterization of stable (2+1)D bright solitons due to simultaneous contributions of the fifth- and seventh-order susceptibilities with suppressed third-order refractive nonlinearity. The images obtained using the SLIM illustrating the laser beam pathway in the quintic-septimal medium show undoubtedly the propagation of (2+1)D solitons for approximately 10 Rayleigh lengths. Good agreement between the experimental and the numerical results based on the optical beam NL propagation equation was observed for all intensities studied.

ACKNOWLEDGMENTS

We acknowledge financial support from the Brazilian agencies Conselho Nacional de Desenvolvimento Cientifico e Tecnológico (CNPq) and the Fundação de Amparo à Ciência e Tecnologia do Estado de Pernambuco (FACEPE). The work was performed in the framework of the National Institute of Photonics (INCT de Fotônica) project and PRONEX/CNPq/FACEPE.

[1] R. W. Boyd, *Nonlinear Optics* (Academic Press, New York, 2008); Y. R. Shen, *The Principles of Nonlinear Optics* (Wiley, New York, 1984).

[2] C. Brée, A. Demircan, and G. Steinmeyer, Phys. Rev. Lett. **106**, 183902 (2011); S. Polyakov, F. Yoshino, and G. Stegeman, J. Opt. Soc. Am. B **18**, 1891 (2001); Y. Liu, M. Durand, S. Chen, A. Houard, B. Prade, B. Forestier, and A. Mysyrowicz, Phys. Rev. Lett. **105**, 055003 (2010).

[3] *Self-focusing: Past and Present (Fundamentals and Prospects)*, edited by R. W. Boyd, S. G. Lukishova, and Y. R. Shen, Topics in Applied Physics Vol. 114 (Springer, Berlin, 2009); J. Zeng and B. A. Malomed, Phys. Rev. E **86**, 036607 (2012); Y. S. Kivshar and G. P. Agrawal, *Optical Solitons: From Fibers to Photonic Crystals* (Academic Press, San Diego, CA, 2003).

[4] A. Couairon and A. Mysyrowicz, Phys. Rep. **441**, 47 (2007); W. Liu, S. Petit, A. Becker, N. Aközbek, C. M. Bowden, and S. L. Chin, Opt. Commun. **202**, 189 (2002).

[5] H. Michinel, M. J. Paz-Alonso, and V. M. Pérez-García, Phys. Rev. Lett. **96**, 023903 (2006); D. Novoa, H. Michinel, and D. Tommasini, *ibid.* **105**, 203904 (2010).

[6] K. D. Moll, D. Homoelle, A. L. Gaeta, and R. W. Boyd, Phys. Rev. Lett. **88**, 153901 (2002); L. Mateos, P. Molina, J. Galisteo, C. López, L. E. Bausá, and M. O. Ramírez, Opt. Express **20**, 29940 (2012).

[7] P. Béjot, J. Kasparian, S. Henin, V. Loriot, T. Vieillard, E. Hertz, O. Faucher, B. Lavorel, and J.-P. Wolf, Phys. Rev. Lett. **104**, 103903 (2010); V. Besse, H. Leblond, and G. Boudebs, Phys. Rev. A **89**, 043840 (2014); G. Point, Y. Brelet, A. Houard, V. Jukna, C. Milián, J. Carbonnel, Y. Liu, A. Couairon, and A. Mysyrowicz, Phys. Rev. Lett. **112**, 223902 (2014).

[8] C. Hang, Y. Li, L. Ma, and G. Huang, Phys. Rev. A **74**, 012319 (2006).

[9] H. Kang, G. Hernandez, and Y. Zhu, Phys. Rev. Lett. **93**, 073601 (2004).

[10] Y. Zhang, U. Khadka, B. Anderson, and M. Xiao, Phys. Rev. Lett. **102**, 013601 (2009).

[11] C. Josserand, Phys. Rev. E **60**, 482 (1999); P. Das, M. Vyas, and P. K. Panigrahi, J. Phys. B: At. Mol. Opt. Phys. **42**, 245304 (2009).

[12] T. W. Huang, C. T. Zhou, H. Zhang, and X. T. He, Phys. Plasmas **20**, 072111 (2013).

[13] T. Köhler, Phys. Rev. Lett. **89**, 210404 (2002); M. Marklund and P. K. Shukla, Eur. Phys. J. B **48**, 71 (2005).

[14] X. He and K. Xie, Opt. Appl. **42**, 103 (2012); Y. V. Kartashov, B. A. Malomed, and L. Torner, Rev. Mod. Phys. **83**, 247 (2011); S. Beheshti, K. J. H. Law, P. G. Kevrekidis, and M. A. Porter, Phys. Rev. A **78**, 025805 (2008); P. G. Kevrekidis, G. Theocharis, D. J. Frantzeskakis, and B. A. Malomed, Phys. Rev. Lett. **90**, 230401 (2003); I. Towers and B. A. Malomed, J. Opt. Soc. Am. B **19**, 537 (2002); M. Centurion, M. A. Porter, P. G. Kevrekidis, and D. Psaltis, Phys. Rev. Lett. **97**, 033903 (2006); M. Centurion, M. A. Porter, Y. Pu, P. G. Kevrekidis, D. J. Frantzeskakis, and D. Psaltis, *ibid.* **97**, 234101 (2006).

[15] R. Y. Chiao, E. Garmire, and C. H. Townes, Phys. Rev. Lett. **13**, 479 (1964).

[16] G. I. Stegeman and M. Segev, Science **286**, 1518 (1999).

[17] Y. Kivshar, Nat. Phys. **2**, 729 (2006).

[18] Z. Chen, M. Segev, and D. N. Christodoulides, Rep. Prog. Phys. **75**, 086401 (2012).

[19] M. Peccianti, C. Conti, G. Assanto, A. de Luca, and C. Umeton, Nature **432**, 733 (2004).

[20] J. Yang, P. Zhang, M. Yoshihara, Y. Hu, and Z. Chen, Opt. Lett. **36**, 772 (2011); D. Kip, C. Anastassiou, E. Eugenieva, D. Christodoulides, and M. Segev, *ibid.* **26**, 524 (2001).

[21] M. Tiemann, T. Halfmann, and T. Tschudi, Opt. Commun. **282**, 3612 (2009); H. S. Eisenberg, Y. Silberberg, R. Morandotti, A. R. Boyd, and J. S. Aitchison, Phys. Rev. Lett. **81**, 3383 (1998); R. De La Fuente, A. Barthelemy, and C. Froehly, Opt. Lett. **16**, 793 (1991).

[22] A. Barthelemy, S. Maneuf, and C. Froehly, Opt. Commun. **55**, 201 (1985); J. S. Aitchison, A. M. Weiner, Y. Silberberg, M. K. Oliver, J. L. Jackel, D. E. Leaird, E. M. Vogel, and P. W. E. Smith, Opt. Lett. **15**, 471 (1990).

[23] P. L. Kelley, Phys. Rev. Lett. **15**, 1005 (1965); E. L. Dawes and J. H. Marburger, Phys. Rev. **179**, 862 (1969); J. H. Marburger, Prog. Quantum Electron. **4**, 35 (1975).

[24] A. Pasquazi, S. Stivala, G. Assanto, J. Gonzalo, J. Solis, and C. N. Afonso, Opt. Lett. **32**, 2103 (2007); E. D'Asaro, S. Heidari-Bateni, A. Pasquazi, G. Assanto, J. Gonzalo, J. Solis, and C. N. Afonso, Opt. Express **17**, 17150 (2009); A. Pasquazi, S. Stivala, G. Assanto, J. Gonzalo, and J. Solis, Phys. Rev. A **77**, 043808 (2008).

[25] E. L. Falcão-Filho, C. B. de Araújo, G. Boudebs, H. Leblond, and V. Skarka, Phys. Rev. Lett. **110**, 013901 (2013).

[26] A. S. Reyna and C. B. de Araújo, Phys. Rev. A **89**, 063803 (2014).

[27] A. S. Reyna and C. B. de Araújo, Opt. Express **22**, 22456 (2014).

[28] E. L. Falcão-Filho, C. B. de Araújo, and J. J. Rodrigues, Jr., J. Opt. Soc. Am. B **24**, 2948 (2007); E. L. Falcão-Filho, R. Barbosa-Silva, R. G. Sobral-Filho, A. M. Brito-Silva, A. Galembeck, and C. B. de Araújo, Opt. Express **18**, 21636 (2010).

[29] J. Zeng and B. A. Malomed, Phys. Rev. A **85**, 023824 (2012); R. M. Caplan, R. Carretero-González, P. G. Kevrekidis, and B. A. Malomed, Math. Comput. Simulat. **82**, 1150 (2012); G. Fibich, N. Gavish, and X.-P. Wang, Phys. D **231**, 55 (2007); C. Rogers, B. Malomed, J. H. Li, and K. W. Chow, J. Phys. Soc. Jpn. **81**, 094005 (2012).

[30] K. C. Jorge, R. Riva, N. A. S. Rodrigues, J. M. S. Sakamoto, and M. G. Destro, Appl. Opt. **53**, 4555 (2014).

[31] P. C. Lee and D. Meisel, J. Phys. Chem. **86**, 3391 (1982).

[32] M. A. Garcia, J. Phys. D: Appl. Phys. **44**, 283001 (2011).

[33] A. S. Desyatnikov, D. Neshev, E. A. Ostrovskaya, Y. S. Kivshar, G. McCarthy, W. Krolikowski, and B. Luther-Davies, J. Opt. Soc. Am. B **19**, 586 (2002); L. Jankovic, P. Aboussouan, M. Affolter, G. Stegeman, and M. Katz, Opt. Express **12**, 5562 (2004); W. Man, S. Fardad, Z. Zhang, J. Prakash, M. Lau, P. Zhang, M. Heinrich, D. N. Christodoulides, and Z. Chen, Phys. Rev. Lett. **111**, 218302 (2013).

[34] P. N. Butcher and D. Cotter, *The Elements of Nonlinear Optics* (Cambridge University Press, Cambridge, 1990).

[35] S. Wang and L. Zhang, Comput. Phys. Commun. **184**, 1511 (2013).